

Amplitude and Frequency Spectrum of Thermal Fluctuations of A Translocating RNA Molecule

Henk Vocks[†], Debabrata Panja^{*} and Gerard T. Barkema^{†,‡}

[†] Institute for Theoretical Physics, Universiteit Utrecht, Leuvenlaan 4,
3584 CE Utrecht, The Netherlands

^{*}Institute for Theoretical Physics, Universiteit van Amsterdam, Valckenierstraat 65,
1018 XE Amsterdam, The Netherlands

[‡]Instituut-Lorentz, Universiteit Leiden, Niels Bohrweg 2, 2333 CA Leiden,
The Netherlands

Abstract. Using a combination of theory and computer simulations, we study the translocation of an RNA molecule, pulled through a solid-state nanopore by an optical tweezer, as a method to determine its secondary structure. The resolution with which the elements of the secondary structure can be determined is limited by thermal fluctuations. We present a detailed study of these thermal fluctuations, including the frequency spectrum, and show that these rule out single-nucleotide resolution under the experimental conditions which we simulated. Two possible ways to improve this resolution are strong stretching of the RNA with a back-pulling voltage across the membrane, and stiffening of the translocated part of the RNA by biochemical means.

PACS numbers: 87.15.bd, 87.14.gn, 36.20.-r, 87.15.A-

1. Introduction

New developments in design and fabrication of nanometer-sized pores and etching methods, in recent times, have put translocation at the forefront of single-molecule experiments [1–9], with the hope that translocation may lead to cheaper and faster technology for the analysis of biomolecules. The underlying principle is that of a Coulter counter [10]: molecules suspended in an electrolyte solution pass through a narrow pore in a membrane. The electrical impedance of the pore increases with the entrance of a molecule as it displaces its own volume of solution. By applying a voltage across the pore, the passing molecules are detected as current dips. For nanometer-sized pores (slightly larger than the molecule’s cross-section) the magnitude and the duration of these dips have proved to be rather effective in determining the size and length of these molecules [11].

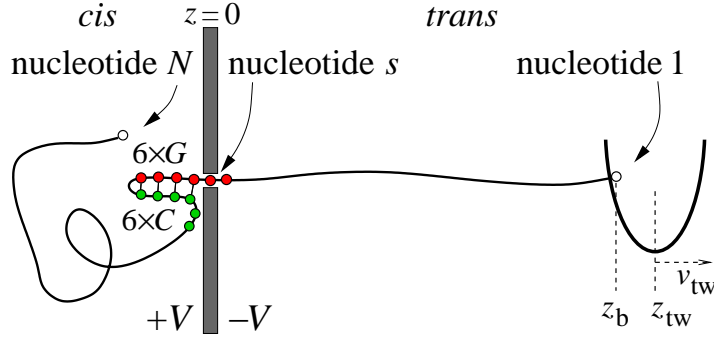


Figure 1. The experiment in schematics, illustrated by only 6 CG-bonds for clarity. An RNA molecule composed of N nucleotides is pulled through a solid-state nanopore in a membrane (placed at $z = 0$) towards the right ($z > 0$) using an optical tweezer, represented by a parabolic potential, at a constant speed v_{tw} . The bottom of the potential is located at z_{tw} ; and the latex bead is located at z_b . The number of monomers located on the *trans*-side of the membrane is called s . The monomers are numbered, starting from the end which is attached to the latex bead; consequently, the nucleotide located in the pore is labelled s . A potential difference $2V$ is also applied across the membrane.

With a membrane placed at $z = 0$, a translocation experiment for determining the secondary structure of an RNA molecule [12–17, 20] composed of N nucleotides proceeds as follows (see Fig. 1). One end of the folded RNA, which is almost completely located on the left (*cis*) side ($z < 0$) of the membrane, is pulled through a solid-state nanopore to the right (*trans*) side ($z > 0$), and a latex bead is attached to nucleotide 1. An optical tweezer captures the bead, and pulls the RNA through the pore at a constant speed v_{tw} . The monomer number at any given time located inside the pore is denoted by s . We denote the voltages on the *cis* and *trans* side by $+V$ and $-V$ respectively; a potential difference $2V$ is thus applied across the membrane, to increase the tension in the translocated part of the RNA so that no secondary structure can form between the tweezer and the pore. During this process, the force exerted by the tweezer on the

RNA is monitored. Since the pore is narrow, for translocation to proceed, the bonds between the basepairs forming the secondary structures must be broken at the pore. The breaking of the basepair-bonds is detected as increased force on the tweezer. The force on the tweezer as a function of time can then be translated into the binding energies of the basepairs as a function of distance along the RNA, yielding a wealth of information on the secondary structure of the RNA.

Note that actual RNA chains may be pulled through the pore either from the 3' or from the 5' end, and the respective force extension curves may pick up both the initial and final location of the stems. From both the force-extension curves, with the help of a probabilistic sequence alignment algorithm [15], one can subsequently reconstruct the base-pairing pattern, the success of which clearly depends on the accuracy with which the arrests in the force-extension curves — as experienced by the tweezer bead — can be tied to the actual translocation coordinates along the backbone of the RNA.

Given that the distances are of nanometer-scale in this experiment, thermal fluctuations of the polymer are expected to blur the arrests of the force extension curves; i.e., blur the coherence between the force exerted by the tweezer and the nucleotide number located in the pore. Since in this experiment one cannot track the events at the pore, the unpredictability of the amount of low-frequency noise in solid state nanopores seem to be the main barrier to progress in this field [18, 19]. The central question addressed in this paper, therefore, is the level of resolution (in units of a nucleotide) that can be achieved by this experiment. All throughout this paper, we define resolution as the accuracy with which the location of secondary structure can be determined along the backbone of the RNA — which is strongly affected by the coherence between the force exerted by the tweezer and the nucleotide number located in the pore. We address this question by studying the amplitude and frequency spectra of the fluctuations at the pore with a combination of theory and computer simulations. The amplitude spectrum determines the resolution limit that can be achieved by ensemble averaging, while frequency spectrum determines the resolution limit that can be achieved by time averaging. Note that the highest resolution that this setup can achieve depends on which of these two limits is higher; this prompts the study of both the amplitude and the frequency spectra of the fluctuations at the pore. Our study rules out single-nucleotide resolution under the experimental conditions which we simulated. Two possible ways to improve this resolution are strong stretching of the RNA with a back-pulling voltage across the membrane, and stiffening of the translocated part of the RNA by biochemical means.

A related problem was considered by Thompson and Siggia [20], who studied whether a measurable signal can be obtained by pulling apart a DNA or RNA molecule by an atomic-force microscope. They formulated their theoretical analysis using an (equilibrium) partition sum that involved the interaction energy between the unzipped strands. In the case of pulling apart a molecule by translocation, the unzipped strands of the molecule are separated by an impenetrable membrane, so the unzipped strands cannot interact directly unless one of the strands translocates through the pore; i.e.,

the process of unzipping *cannot* be decoupled from the dynamics of translocation. Consequently, the method of Thompson and Siggia cannot be easily imported to study our setup. We also note that recently a number of researchers, e.g., Sauer-Budge *et al.* [21] and Bockelmann *et al.* [22] have studied the case of pulling apart a molecule by translocation: however, their formulations do not take into account any dynamics of translocation, and therefore they only provide a simplified analysis of the problem. Given that the (anomalous) dynamics of translocation involves long memory effects [27–31], we follow a different method in this paper; this allows us to study the full dynamic problem (i.e., including the frequency spectrum of the thermal fluctuations).

Our work is related to the study of Bundschuh *et al.* [16] of translocation of RNA or DNA through a nanopore, describing slow and fast regimes of translocation: for the former, the *cis* side of the RNA molecule essentially remains equilibrated at almost all times, while for the latter, the base-pairing pattern on the *cis* side is essentially frozen during unzipping. Our analysis describes a maximum pulling velocity of the optical tweezer that allows the *trans* side of the molecule enough time to always remain in its steady state, thereby providing the quantitative distinguishing characteristics between the two regimes described by Bundschuh *et al.*

The structure of this paper is as follows. In Sec. 2, we describe our computer model. In Secs. 3 and 4, we analyse the problem without and with thermal fluctuations respectively. In Sec. 5 we conclude the paper with a discussion on the results.

2. Computer model

We model the RNA with N nucleotides as a lattice polymer with N monomers on a face-centred-cubic lattice. Multiple occupation of the same site is forbidden, i.e., the polymer is described by a self-avoiding-walk. For practical purposes, this restriction is lifted for consecutive nucleotides along the chain. The dynamics of the polymer consists of single-nucleotide hops to nearest-neighbour sites, attempted at random with rate unity, and accepted with Metropolis probabilities. This model [23–26] describes both reptation and Rouse moves, but does not include explicit hydrodynamics. We have used this model successfully to simulate polymer translocation under various circumstances [27–31]. Since our model is a variant of a freely-jointed-chain, we expect it to reproduce poly(U) RNA behaviour reasonably well [32].

In translocation experiments with biological nanopores, e.g., alpha-haemolysin, the polymer might show sequence-specific binding and unbinding to the pore wall [6, 7, 33]. Such interactions between the polymer and the membrane are not expected to play a role in experiments of translocation through a solid-state nanopore, as used in the experiments of Refs. [8, 9]. It has also been suggested that the translocation of single-stranded DNA through alpha-haemolysin nanopore is direction specific [34] (3' to 5' as opposed to 5' to 3'); in the same paper, by computer simulations, the authors demonstrated that such direction-specificity should not be present when the pore diameter is $\gtrsim 1.5$ nm. Given that the typical diameters for solid-state nanopores are

$\gtrsim 2$ nm [35], in our simulations, we neglect interactions between the polymer and the membrane, other than excluded-volume interactions (i.e., the polymer cannot cross the membrane other than through the pore).

Since we want to study how secondary structure influences the translocation process, we add the ability for parts of the polymer to form two hairpins. The real RNA sequence which comes closest to our approach is a poly(U) RNA with a sequence composition $U_{30}(U_{60}G_{32}U_6C_{32})_2U_{60}$, wherein *each nucleotide corresponds to a monomer*: two C and G -nucleotides on neighbouring lattice sites can form a bond with an affinity $E_{CG} = 2.3 k_B T$, but we do not allow GU pairing. The latter is a simplification from how a real RNA molecule with the above sequence would behave, but with this simplification we *a priori* know what to expect for the secondary structure of this polymer — namely two hairpins, each with 32 CG -bonds [36] — on which we study the effect of thermal noise that limit the achievable basepair resolution of the secondary structures.

Our model of the optical tweezer is that the latex bead, i.e., nucleotide 1 feels a spherically symmetric harmonic trap with spring constant k_{tw} , centred around the location of the optical tweezer at a distance z_{tw} from the membrane.

It is clear that our model does not capture the full details of a real laboratory experiment: indeed a more detailed model could include explicit hydrodynamics, detailed RNA interactions such as GU pairing, and a more elaborate description of the charge distributions on the RNA. Leaving out explicit hydrodynamics does alter polymeric motion (from Zimm to Rouse dynamics) and therefore is likely to affect the polymer's memory effects. Although at this moment we do not precisely know how the memory effects that are relevant for the present problem — discussed in Sec. 4 — will alter when explicit hydrodynamics are incorporated, the low-frequency domination of the memory effects will not disappear.

To correspond to experimental parameters we use a lattice spacing of $\lambda = 0.5$ nm, comparable to the persistence length (as well as the typical inter-nucleotide distance) for poly(U) [37]. The resulting forces measured at the tweezer are 60 pN or less, similar to experimental values [37]. Equating the diffusion coefficient 2.5×10^{-6} cm²/s for U_6 [38] to that of a polymer of length $N = 6$ in our model, one unit of time in our simulations corresponds roughly to 100 ps. The tweezer velocity is one lattice spacing λ per 300,000 units of time, or ~ 20 μ m/s, comparable to typical experimental velocities. The time scale λ/v_{tw} is larger than that (or of the order) of the longest time-scale of the translocated part of the RNA, implying that *the translocated part of the RNA can be treated as properly thermalised at all times*. In our simulations, the value of $\Delta U = 2qV$ ranges from 0.4 to $2.75 k_B T$. Given that at room temperature $k_B T = 25$ meV and assuming that each nucleotide carries an effective charge around $q = 0.5$ times the electron charge (due to Manning condensation, which limits the charge to one electron charge per Bjerrum length[‡]) [40], our simulations correspond to an experimentally

[‡] Due to Manning condensation, the effective charge per unit length is limited to approximately one electron charge per Bjerrum length. In water, the Bjerrum length is about 7 Å. Since the typical RNA base pair distance is ≈ 3.4 Å, the effective charge is approximately $0.5e$ per nucleotide. In the pore, the

applied voltage differences ranging from $10 \text{ mV} < V < 70 \text{ mV}$.

A typical simulation output is presented in Fig. 2. It consists of the force $F_{\text{tw}}(t)$ exerted by the optical tweezer as a function of time: *this information is readily accessible in real experiments*. In our simulations, we also monitor the number s of monomer located in the pore as a function of time: *this information is typically not accessible in real experiments*. In the simulation of figure 2, the force exerted by the tweezer hovers around a fixed strength $3.4 k_B T / \lambda$ (approximately 30 pN), except between $t = 1.4 \times 10^7$ to 3.4×10^7 resp. $t = 4.6 \times 10^7$ to 6.7×10^7 , when the first and second hairpins are pulled through the pore. Indeed, the top panel of Fig. 2 shows that at the onset of these intervals, $s(t)$ is almost constant, around 90 and 220, the starting locations of the hairpins.

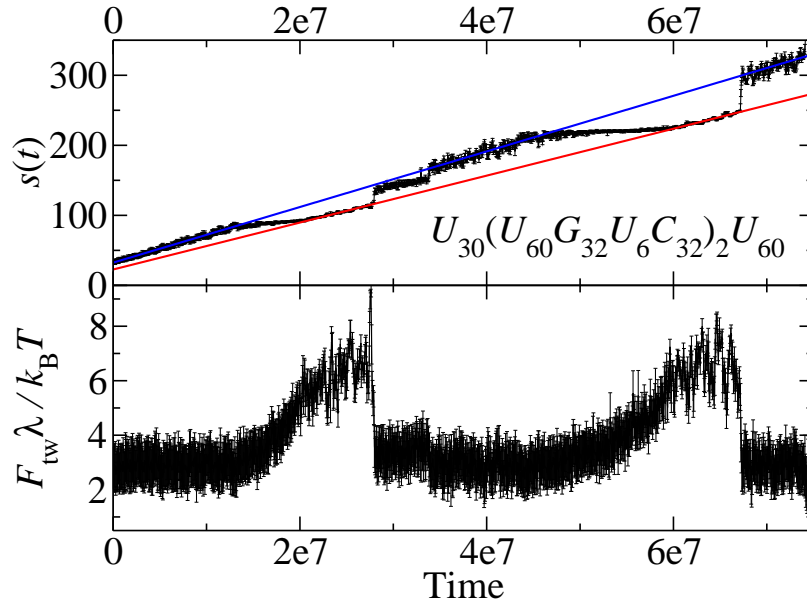


Figure 2. Upper panel: nucleotide in the pore s as a function of time for a poly(U) RNA of composition $U_{30}(U_{60}G_{32}U_6C_{32})_2U_{60}$, pulled with constant velocity $v_{\text{tw}} = \lambda$ per 300,000 time steps (approximately $20 \mu\text{m/s}$). The binding energy of each bond is set to $E_{CG} = 2.3 k_B T$, with $2qV = 1.5 k_B T$. Every data point is an average of 1500 consecutive measurements each 100 time steps apart, with the standard deviation represented by the error bars. The two straight lines are guides for the eye. Lower panel: the corresponding chain tension measured by means of the optical tweezer, with $k_{\text{tw}} = 1 k_B T / \lambda$.

dielectric constant is significantly lower than that of water, consequently the Bjerrum length (which is inversely proportional to the dielectric constant) is much larger, and hence the effective charge is much lower (a tenth of an electron charge per nucleotide or even less [21, 39]). For our work, a key quantity is the stretching force, determined by the energy difference across the pore, set by the effective charge in solution. Thus, for our purpose, the relevant effective charge is $0.5e$ per nucleotide. The main consequence of the much lower effective charge inside the pore is that RNA is less eager to enter the pore, but that has no consequences for this work.

3. Translocation without thermal fluctuations

First we discuss what sort of information on the secondary structure can *ideally* — i.e., in the *absence* of thermal fluctuations — be obtained from $F_{\text{tw}}(t)$. We do this under the assumptions that the force extension curve of the RNA without any secondary structure is sequence-independent, and that the tweezer velocity is low enough for the force exerted by the tweezer to maintain a uniform chain tension ϕ all along the translocated part of the RNA. Then, ϕ is uniquely determined by the relative extension $x = z_{\text{b}}/s$, and is balanced by $F_{\text{tw}}(t)$, i.e.,

$$\phi = \mathcal{F}(x) = F_{\text{tw}} = k_{\text{tw}}(z_{\text{tw}} - z_{\text{b}}), \quad (1)$$

where k_{tw} is the stiffness of the optical tweezer. Additionally, the equality of the rate of work done by the tweezer and the gain in free energy by the translocating nucleotides at the pore yields

$$F_{\text{tw}} dz_{\text{b}} = (\Delta U - T\Delta S) ds, \quad (2)$$

where ΔS is the entropic cost per nucleotide translocation due to the imbalance of the (entropic) chain tension across the pore, and ΔU is the energetic cost per nucleotide translocation. If translocation of the nucleotides does not involve breaking of CG -bonds at the pore, then $\Delta U = \Delta U_c \equiv 2qV$, otherwise $\Delta U = \Delta U_b \equiv 2qV + E_{CG}$. Thus, given z_{b} and $(\Delta U - T\Delta S)$, Eqs. (1) and (2) determine both the tweezer force and the relative extension.

During the translocation of the first 90 nucleotides of $U_{30}(U_{60}G_{32}U_6C_{32})_2U_{60}$, no secondary structure is broken at the pore — consequently, $\Delta U = \Delta U_c$ — and the tweezer force remains constant at $F_{\text{tw}}(t) = 3.4 k_{\text{B}}T/\lambda$ (approximately 30 pN). The speed of translocation is then given solely by Eq. (1), with $\dot{z}_{\text{b}} = v_{\text{tw}}$, as $\dot{s} = v_{\text{tw}}/\mathcal{F}^{-1}[F_{\text{tw}}(t)] = 1$ nucleotide per 252,000 time steps, for which we have used the numerically obtained force extension curve (inset, Fig. 3); this speed \dot{s} is shown in Fig. 2 by the upper (blue) line.

Following the arrival of the first hairpin at the pore, translocation requires breaking of the CG -bonds, and consequently, ΔU increases by $E_{CG} = 2.3 k_{\text{B}}T$. Both the tweezer force and the relative extension adjust to new values, determined by Eqs. (1) and (2) for the new value for ΔU . The resulting tweezer force equals $F_{\text{tw}}(t) = 7.5 k_{\text{B}}T/\lambda$ (approximately 70 pN); the correspondingly adjusted speed \dot{s} is shown in Fig. 2 by the lower (red) line.

After the translocation of the first 32 G -nucleotides, ΔU returns to its base value ΔU_c . The tweezer force and the relative extension, too, fall back to their pre-hairpin values. This is seen in Fig. 2 by $s(t)$ leaving the lower red line *sharply* to re-coincide with the upper blue line; i.e., quite a few nucleotides at the end of the hairpin translocate nearly immediately. This chain of events repeats itself during translocation of the second hairpin: first the tweezer force increases gradually to its higher value and the translocated distance approaches the lower red line, then the tweezer force decreases steeply to its lower value and the translocated distance jumps to the upper blue line.

In conclusion, most features of Fig. 2 are qualitatively well-understood. The above framework can be easily extended to a wider set of bond strengths and more elaborate secondary structures. Without thermal fluctuations, the setup is perfectly suited to determine the secondary structure up to the nucleotide resolution, under the restriction that the consecutive bonds along the backbone of the RNA are of increasing strength; if strong bonds are followed by weaker bonds that are not strong enough to halt the translocation process, the breaking of the weaker bonds will not be accompanied by an increase of F_{tw} and the experiment will reveal little information about these weaker bonds.

4. Translocation with thermal fluctuations

In reality, thermal fluctuations are omnipresent in this nano-scale experiment, and as argued earlier, for solid-state nanopores they are the dominant source of noise at the pore. In fact, it is precisely the (thermal) fluctuations in $s(t)$ that serve to blur the coherence between $F_{\text{tw}}(t)$ and $s(t)$, and thereby limit the resolution that can be achieved by this experiment. We will now study both the amplitude and the frequency spectrum of these thermal fluctuations in $s(t)$.

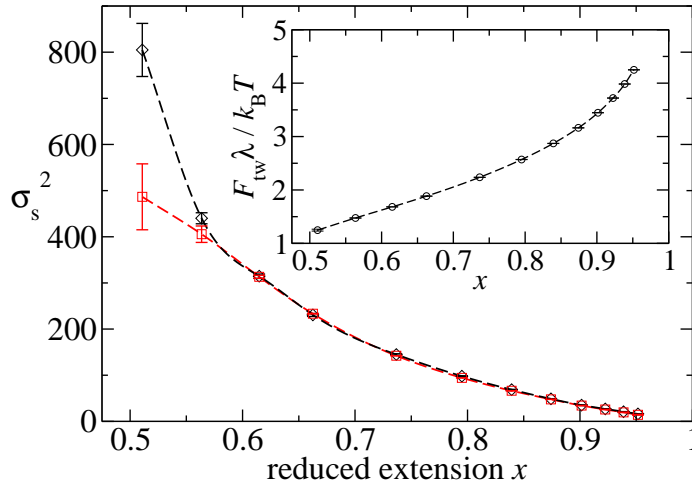


Figure 3. σ_s^2 , the mean square displacement of s vs. reduced extension $x = z_b/s$, at constant $z_{\text{tw}} = 300 \lambda$. The chain tension ϕ is slowly increased by changing $\Delta U = 2qV$ from 0.40 to $2.75 k_B T$. Each data point required 80 independent polymers and simulation times of 20 million time steps, with a measurement every 100 time steps. Data points from direct simulations and Eq. (3) are represented as black diamonds and red squares. The dashed lines are cubic splines. The error bars represent statistical errors only. Inset: Rescaled force-extension curve for our model.

The amplitude $\sigma_s(t, \Delta U)$ of the fluctuations in $s(t)$ is that of an entropic spring at fixed extension z_b with one end tethered at the tweezer, while the number of nucleotides in the spring are allowed to fluctuate through the pore. Now consider a *different* problem — an entropic spring with an average, but fluctuating extension z_b . From

the equipartition theorem, these fluctuations are given by $\langle \delta z_b^2 \rangle = k_B T / c_{z_b}$ [with spring constant $c_{z_b} = (\partial \mathcal{F} / \partial z_b)_s = \mathcal{F}'(x) / s$, in which $x = z_b / s$ is the relative extension]. For the present problem, such fluctuations in z_b can be thought of to be mediated by the fluctuations in s , yielding [41]

$$\sigma_s^2(t, \Delta U) = \langle \delta z_b^2 \rangle \left[\frac{\partial s}{\partial z_b} \right]_x^2 = s(t) [x^2 \mathcal{F}'(x)]^{-1} k_B T. \quad (3)$$

In Fig. 3, Eq. (3) is compared to the simulation results for several values of ΔU , with constant $z_{tw} = 300 \lambda$. Note that ΔU only serves to set the value of ϕ . Of practical importance is the observation that according to Eq. (3) the amplitude of the thermal fluctuations decreases with increasing tension. Thus, an increase of the applied voltage difference will reduce the thermal fluctuations in s thereby increasing the resolution of the secondary structure determination. The same effect can also be achieved by increasing the chain stiffness, thereby increasing $\mathcal{F}'(x)$. In practice, this could for instance be realised through chemical means. For instance, it is known that the salinity affects the chain stiffness [37]. Also, certain proteins (such as RecA for ssDNA) can be added on the trans-side of the membrane, to increase the chain stiffness dramatically, while at the same time reducing secondary structure formation on the side of the tweezer.

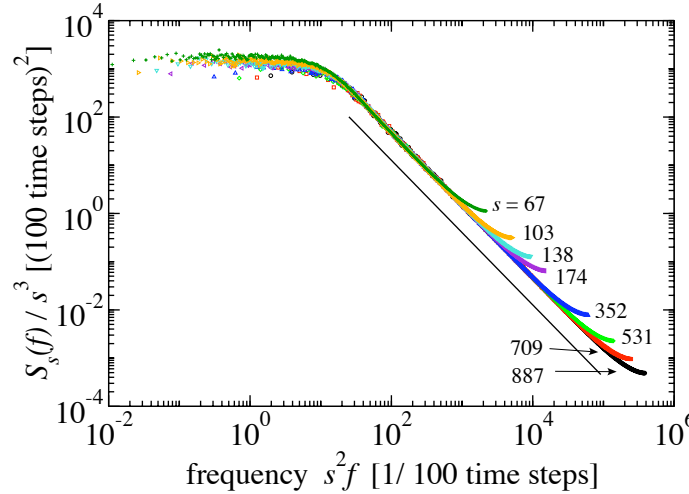


Figure 4. (Rescaled) power spectrum of $s(t)$, $S_s(f)$, versus (rescaled) frequency for $\Delta U = 1.5 k_B T$, and $z_{tw}/\lambda = 60, 90, 120, 150, 300, 450, 600, 750$. Each curve is composed of statistics from 80 polymers for 40 million time steps, the value of s corresponding to each curve are shown in the Figure. The solid line $\sim f^{-3/2}$ is added as a guide to the eye. The unit of $s^2 f$ along the horizontal axis, $1/100$ time steps, is approximately equal to 100 MHz.

For the frequency spectrum of $s(t)$, we return to Ref. [30]. Therein we showed that $\dot{s}(t)$ and the chain tension imbalance across the pore are related via a time-dependent

memory kernel $a(t)$. This result, adapted to the notations in this paper, is given by

$$\dot{s}(t) = \int_{-\infty}^t dt' a(t-t') [\phi(t') - \phi_{z<0}(t')], \quad (4)$$

where $\phi_{z<0}$ is the chain tension of the RNA at the $z < 0$ side of the pore, and $a(t) \sim t^{-3/2} \exp[-t/\tau_{\mathcal{F}}]$; thus, the memory kernel $a(t)$ is described by a power-law decay with exponent $-3/2$, up to some cut-off time $\tau_{\mathcal{F}}$; this cut-off time is found to increase quadratically with the length of the translocated RNA: $\tau_{\mathcal{F}} \sim s^2$ [30]. The immediate consequence of Eq. (4) is that

$$\langle \dot{s}(t) \dot{s}(t') \rangle \sim |t - t'|^{-3/2} \exp[-|t - t'|/\tau_{\mathcal{F}}], \quad (5)$$

following the fluctuation-dissipation theorem [42], i.e.,

$$\begin{aligned} \langle s(t) s(t') \rangle &= \int_0^t dt_1 \int_0^{t'} dt_2 \langle \dot{s}(t_1) \dot{s}(t_2) \rangle \\ &= \begin{cases} 4 [|t - t'|^{1/2} - |t|^{1/2} - |t'|^{1/2}] & |t - t'| \lesssim \tau_{\mathcal{F}} \\ C & |t - t'| \gg \tau_{\mathcal{F}} \end{cases}, \end{aligned} \quad (6)$$

with some constant C . This autocorrelation function, for $|t - t'| \lesssim \tau_{\mathcal{F}}$, has the same form as that of a fractional Brownian motion (FBM) [43, 44]

$$\langle s(t) s(t') \rangle = C_1 (|t|^{2H} + |t'|^{2H} - |t - t'|^{2H}), \quad (7)$$

with Hurst parameter $H = 1/4$, and some constant C_1 . Since the r.h.s. of Eq. (7) is not a function of $(t - t')$ alone, the spectral density of the FBM is not well-defined. However, by applying generalised concepts such as the Wigner-Ville spectrum [43], a limiting power spectrum can be obtained as follows: $S_s(f) = \frac{C_2}{|f|^\alpha}$, with $\alpha = 2H + 1 = 3/2$, with some constant C_2 . We therefore expect a power spectrum, with $f_c \sim 1/\tau_{\mathcal{F}} \sim 1/s^2$,

$$S_s(f) = \begin{cases} \frac{C_2}{|f|^{3/2}} & (|f| > f_c) \\ \frac{C_2}{f_c^{3/2}} & (|f| < f_c) \end{cases}. \quad (8)$$

As shown in Fig. 4, after having rescaled $S_s(f)$ and f by s^{-3} and s^2 respectively, the collapse of the power spectra confirms Eq. (8). The spectrum is dominated by the low frequency fluctuations of $s(t)$, which are not easily suppressed by time averaging.

The translocated part of the RNA can be considered to be in a steady state as long as $\dot{s}(t) < \tau_{\mathcal{F}}^{-1}$, i.e., the time between the passage of consecutive nucleotides through the pore does not exceed the time for the longest memory in the translocated part of the RNA. This time for the longest memory is set by the longest length s_{\max} of the translocated part of the RNA. If the tweezer is pulled with a velocity exceeding

$$v_{\text{tw},\max}(t, \Delta U) = x \cdot f_c \sim \frac{C_2^2 x^5 \mathcal{F}'(x)^2}{s_{\max}^2 (k_B T)^2}, \quad (9)$$

where Parseval's theorem has been used to equate Eq. (8) to Eq. (3), the *trans* side of the molecule is not allowed enough time to reach the steady state. This results in forces at the tweezer that far exceed the forces required to pull monomers through the pore at steady state (of the molecule on the *trans* side). Fig. 4 shows that if a

potential difference of $\Delta U = 1.5k_B T$ is applied, the power rescaled spectrum crosses over from a frequency-independent regime to a power-law regime if $s^2 f = 0.1$ to 0.15 ; with a pulling velocity $v_{\text{tw}} = \lambda/300,000$ (roughly $\sim 20 \mu\text{m/s}$) the typical frequency is $f \sim 300,000^{-1} \approx 0.3 \text{ MHz}$; the rescaled quantity $s^2 f$ then reaches the crossover once the translocated part of the chain has a length $s_{\text{max}} \approx 200$ nucleotides. Beyond this length, the translocated part of the chain will be pulled out of its equilibrium shape, and the force felt by the tweezer is no longer determined by what happens near the pore, but rather by what happens in the translocated part of the chain, with the consequence that limited information about possible secondary structure will be obtained. In targeted simulations we have indeed observed the behaviour that *without* any base-pairing, for tweezer velocities higher than $\lambda/300,000$ ($\approx 20 \mu\text{m/s}$), the force at the tweezer is an increasing function of time significantly once $s_{\text{max}} \approx 200$ has been reached.

5. Discussion and conclusions

Having demonstrated the importance of thermal fluctuations in $s(t)$, let us now revisit the translocation of $U_{30}(U_{60}G_{32}U_6C_{32})_2U_{60}$, cf. Fig. 2. Except between times 1.4 and 3.4×10^7 (resp. 4.6 and 6.7×10^7), $F_{\text{tw}}(t)$ is roughly $3.4 k_B T/\lambda$ (approximately 30 pN), with fluctuations $\langle \Delta F_{\text{tw}}^2(t) \rangle \approx k_{\text{tw}} k_B T$, while Eq. (3) explains the growth of $\sigma_s^2(t)$ linearly with $s(t)$ (hence linearly with t). It is important to stress that while the fluctuations in $F_{\text{tw}}(t)$ may be removed to a reasonable degree by time averaging (e.g., by reducing the velocity of the tweezer), the fluctuations in $s(t)$ fundamentally reduce the accuracy with which RNA secondary structure can be observed. As soon as the hairpin is within a distance of order $\sigma_s(t, \Delta U)$ from the pore, i.e., $\langle s(t) \rangle + \sigma_s(t, \Delta U_c) = 90$ (resp. 220), the tweezer force increases already, to reach a plateau once $\langle s(t) \rangle - \sigma_s(t, \Delta U_b) = 90$ (resp. 220). Translocation at the pore then proceeds with a constant rate $v_{\text{tw}}/\mathcal{F}^{-1}(F_{\text{tw}})$, until $\langle s(t) \rangle + \sigma_s(t, \Delta U_b) = 122$ (resp. 252) (in which we assume that the effective affinity E_{CG} is not altered much as the unzipping of the hairpin proceeds), at which time the chain tension is released by rapid translocation of the remaining nucleotides. These considerations clearly establish that only secondary structure elements with at least two times $\sigma_s(t, \Delta U_b)$ basepairs can be detected accurately, assuming that the affinities of consecutive basepairs are more or less alike. With the choice of parameters in the simulations leading to Fig. 2 which are comparable to typical experimental values, this means that the resolution is limited to ≈ 8 nucleotides. Information on smaller lengths is washed out by the thermal fluctuations, making it very hard to retrieve. Moreover, the basepairs of the preceding stem of the secondary structure must be characterised either by weaker affinities, or by strong heterogeneity.

Although the fluctuations in $s(t)$ are not easily suppressed, Eq. (3) does leave open avenues for higher accuracy, either by increasing the relative extension $x = z_b/s$, or by increasing the stiffness $\mathcal{F}(x)$ of the polymer on the trans side of the membrane. The former can be achieved by applying a stronger potential difference $2V$ (the strength

of which is of course limited by experimental considerations). On the other hand, the polymer's stiffness can be actively enhanced, e.g., by altering the salinity of the solution [37]; alternatively, if one is interested in doing single-molecule experiments with ssDNA, the addition of RecA proteins to the solution only on the trans of the membrane may be of help as well (this will increase the stiffness of the polymer on the trans side of the membrane, but since these proteins cannot pass through the pore, the secondary structure on the cis side will be left unaffected).

If biological pores such as alpha-haemolysin are used for this experiment instead of solid-state nanopores, the translocating polymer will show sequence-dependent binding/unbinding to the pore wall. Although we cannot oversee all consequences of such interactions, we do not expect these to affect the coherence between the force felt at the tweezer and the translocated length, nor the frequency spectrum of the fluctuations in the translocated part of the chain. Hence, our conclusions should also apply to biological pores.

Acknowledgement

We acknowledge useful discussions with our experimental colleagues Cees Dekker and Nynke Dekker at Delft University of Technology, The Netherlands. D. P. gratefully acknowledges ample computer time at the Dutch national supercomputer facility SARA.

- [1] J. J. Nakane, M. Akeson, and A. Marziali, *J. Phys.: Condens. Matter* **15** R1365 (2003).
- [2] J. J. Kasianowicz *et al.*, *Proc. Natl. Acad. Sci. USA* **93** 13770 (1996).
- [3] S. E. Henrickson *et al.*, *Phys. Rev. Lett.* **85**, 3057 (2000).
- [4] A. Meller, L. Nivon, and D. Branton, *Phys. Rev. Lett.* **86**, 3435 (2001).
- [5] M. Akeson *et al.*, *Biophys. J.* **77**, 3227 (1999).
- [6] A. Meller *et al.*, *Proc. Natl. Acad. Sci. USA* **97**, 1079 (2000).
- [7] A. Meller, and D. Branton. *Electrophoresis* **23**, 2583 (2002).
- [8] A. J. Storm *et al.*, *Nano Lett.* **5**, 1193 (2005).
- [9] U. F. Keyser *et al.* *Nature Physics* **2** 473 (2006).
- [10] W. H. Coulter. 1953. Means for counting particles suspended in a fluid. *U.S. Patent 2,656,508*.
- [11] J. W. F. Robertson *et al.* *Proc. Nat. Acad. Sci. USA* **104**, 8207 (2007), and the references therein.
- [12] M. Rief *et al.*, *Science* **276**, 1109 (1997).
- [13] J. Liphardt *et al.*, *Science* **292**, 733 (2001).
- [14] B. Onoa *et al.*, *Science* **299**, 1892 (2003).
- [15] U. Gerland, R. Bundschuh, and T. Hwa. *Phys. Biol.* **1**, 19 (2004).
- [16] R. Bundschuh, and U. Gerland, *Phys. Rev. Lett.* **95**, 208104 (2005).
- [17] S. Kotsev, and A. B. Kolomeisky, *J. Chem. Phys.* **125** 084906 (2006).
- [18] R. M. M. Smeets, *DNA and ion transport through solid-state nanopores*. Ph.D. thesis, Delft University of Technology, The Netherlands (2008).
- [19] R. M. M. Smeets *et al.*, *Proc. Natl. Acad. Sci. USA* **105**, 417 (2008).
- [20] R. E. Thompson, and E. D. Siggia, *Europhys. Lett.* **31** 335 (1995).
- [21] A. F. Sauer-Budge *et al.*, *Phys. Rev. Lett.* **90**, 238101 (2003).
- [22] U. Bockelmann and V. Viasnoff, *Biophys. J.* **94**, 2716 (2008).
- [23] A. van Heukelum *et al.*, *J. Chem. Phys.* **119**, 8197 (2003).
- [24] A. van Heukelum *et al.*, *Macromolecules* **36**, 6662 (2003).

- [25] J. Klein Wolterink *et al.*, *Macromolecules* **38**, 2009 (2004).
- [26] J. Klein Wolterink and G.T. Barkema, *Mol. Phys.* **103**, 3083 (2005).
- [27] D. Panja, G. T. Barkema, and R. C. Ball, e-print arXiv:cond-mat/0610671.
- [28] D. Panja, G. T. Barkema, and R. C. Ball, *J. Phys.: Condens. Matter* **19**, 432202 (2007).
- [29] D. Panja, G. T. Barkema, and R. C. Ball, *J. Phys.: Condens. Matter* **20** 075101 (2008).
- [30] D. Panja and G. T. Barkema, *Biophys. J.* **94**, 1630 (2008).
- [31] H. Vocks *et al.*, *J. Phys.: Condens. Matter* **20**, 095224 (2008).
- [32] Y. Seol, G. M. Skinner, and K. Visscher, *Phys. Rev. Lett.* **98**, 158103 (2007).
- [33] O. V. Krasilnikov, C. G. Rodrigues, and S. M. Bezrukov, *Phys. Rev. Lett.* **97**, 018301 (2006).
- [34] J. Mathé *et al.* *Proc. Natl. Acad. Sci. USA* **102**, 12377 (2005).
- [35] C. Dekker, *Nature Nanotech.* **2**, 209 (2007); M. Wanunu *et al.*, *Biophys. J.* **95** 4716 (2008).
- [36] Note here that the sequence $U_{30}(U_{60}G_{32}U_6C_{32})_2U_{60}$ has a prominent alternative structure (besides two hairpins): one long hairpin with a loop of size 60. Such a loop of size 60 is often observed within our polymer model. However, in our polymer model secondary structures tend to be highly compactified, which makes it difficult to provide a quantitative comparison with real RNA chains.
- [37] Y. Seol, G. M. Skinner, and K. Visscher, *Phys. Rev. Lett.* **93**, 118102 (2004).
- [38] I.-C. Yeh and G. Hummer, *Biophys. J.* **86**, 681 (2004).
- [39] J. Zhang and I. Shlovskii, *Phys. Rev. E* **75**, 021906 (2007).
- [40] *Soft condensed matter physics in molecular and cell biology.* W.C.K. Poon and D. Andelman (eds), CRC Press, Boca Raton, USA, 2006.
- [41] The direct simulation results and Eq. (3) in Fig. 3 deviate from each other for $x \lesssim 0.6$, since in this case the assumption $\sigma_s \ll s$ does not hold any more. Also, tethering of nucleotide 1 requires $k_{tw} \gg c_{zb}$; this assumption is clearly valid in our simulations, but need not be valid in real experiments.
- [42] Note here that Ref. [30] is about pulling the tweezer with a constant force, while in this paper the tweezer is pulled with a constant velocity. This does not affect the memory kernel and the consequences of the RNA's memory.
- [43] C. Heneghan, and G. McDarby, *Phys. Rev. E* **62**, 6103 (2000).
- [44] H. E. Hurst, *Trans. Am. Soc. Civ. Eng.* **116**, 770 (1951).